Geophys. J. Int. (2003) **155,** 1042–1050

Dynamic branching, arresting of rupture and the seismic wave radiation in self-chosen crack path modelling

Nobuki Kame[1]* and Teruo Yamashita[2]

[1]*Department of Earth and Planetary Sciences and Division of Engineering and Applied Sciences, Harvard University, Cambridge,* MA 02138*, USA. E-mail: kame@esag.harvard.edu*

[2]*Earthquake Research Institute, University of Tokyo,* 1-1-1 *Yayoi, Bunkyo-ku, Tokyo* 113-0032*, Japan*

Accepted 2003 August 29. Received 2003 August 18; in original form 2002 July 4

SUMMARY

We simulate spontaneous mode II crack propagation for which the path is dynamically self-chosen. Our main interests are in the formation of the branching path under the influence of self-radiating wave stresses, and in the resultant seismic wave radiation. For these purposes, we adopt the elastodynamic boundary integral equation method (BIEM), which does not impose any constraints on the crack path. We consider a crack subjected to biaxial compression, on which Coulomb friction acts and we determine the extension and the direction of crack growth from a critical shear stress criterion. Our analysis shows that the crack tip bifurcates into two branches at the high-speed propagation stage due to the stress wave localization near the crack tip. Each of the two branches is generated in compressive and tensile stress regions around the propagating tip. Under the same friction coefficient different normal stresses cause different friction levels on them and that results in increasing their bending angles asymmetrically. If the angle of bending exceeds a threshold under biaxial compression, the stress to be released on the curved crack branch becomes negative. Therefore, the growth of such branch is arrested after increasing the bending angle. We then synthesize its waveforms to find phases associated with the dynamic branching. We compare them with those emitted by two planar crack models for which the growths are arrested by inhomogeneities in the fracture strength or the pre-stress state: little effect appeared from the branching characteristics in the waveforms. This is because the curved branches themselves make little contribution to the wave radiation due to the negligible slip velocity.

Key words: cracks, elastodynamics, fractures, rupture propagation, seismic waves.

1 INTRODUCTION

It is increasingly clear that surface traces of large earthquakes are not simply planar but show some typical geometrical structures such as bends, branches and steps (e.g. Sieh *et al.* 1993; Barka 1999). Underground complexity is inferred geodetically by the newly developed remote sensing techniques such as GPS and inSAR as well as classical triangular surveying (e.g. Kanamori 1972; Massonnet *et al.* 1993; Yoshida *et al.* 1996). Geometrical complexity is also inferred seismologically by examining detailed recordings and precise aftershock relocations (e.g. Felzer & Beroza 1999). The dynamic formation of such geometrical complexity has been assumed to be related to strong ground motion or arresting of dynamic faulting (e.g. King & Nabelek 1985; Umeda 1990).

*On leave from: Department of Earth and Planetary Sciences, Kyushu University, 6-10-1 Hakozaki, Higashi-ku, Fukuoka 812-8581, Japan. E-mail: kame@geo.kyushu-u.ac.jp

On the other hand, theoretical analyses have shown the branching instabilities in 2-D crack propagation (e.g. Yoffe 1951; Freund 1989). The solutions revealed that angular distribution of 'hoop traction' around a fast propagating crack tip is strongly distorted by wave stresses to concentrate in the off-plane direction rather than on-plane when the rupture speed exceeds the 'critical speed' $c_{\rm crt}$ (see Figs 1 and 2). The critical speed is approximately $0.77c_{\rm s}$ for mode II deformation, where $c_{\rm s}$ is the shear wave speed (see the Appendix). It has long been suggested that these high off-plane stresses could play a central role in branching of fracture paths (e.g. Rice 1980). The theoretical analyses are, however, limited to a rupture remaining on a plane before branching mainly because of the necessity of mathematical simplicity. The whole dynamics including the branching process still remains unclear and numerical methods are therefore required for the analysis of crack paths with geometrical complexity.

Recent progress in the development of numerical methods enabled us to handle dynamic formation of non-planar crack paths. Xu & Needleman (1994) calculated the spontaneous bifurcation for a mode I crack under a sudden tensile load using the finite-element

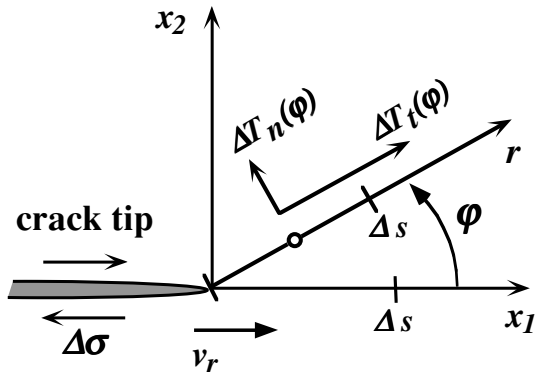

Figure 1. Incremental hoop shear and normal tractions ($\Delta T_t(\varphi)$, $\Delta T_n(\varphi)$) due to the presence of a crack: they act on an inclined plane originating from a crack tip. The angle φ is measured from the x_1-axis. Δs is a unit length of the boundary element and the open circle represents an evaluation point for $\Delta T_t(\varphi)$ and $\Delta T_n(\varphi)$ in computation.

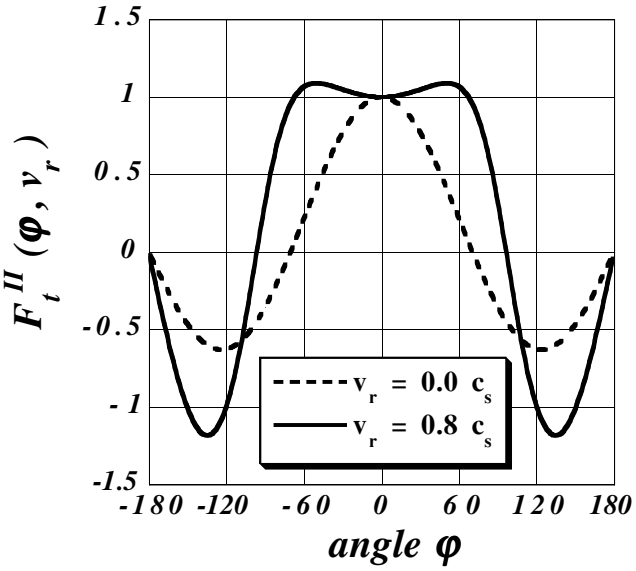

Figure 2. Dynamic crack tip singular stress fields, for right lateral mode II rupture at two different rupture speeds, $v_r = 0.0c_s$, $0.8c_s$. $F_t^{II}(\varphi, v_r)$ represents the angular distribution of the singular component of $\Delta T_t(\varphi)$ (see the Appendix).

method (FEM). The method, however, has a restriction that the crack tip can grow locally only in the directions 0° and ±45°. Seelig & Gross (1999) developed the boundary integral equation method (BIEM) and studied branching of fast running tensile cracks. In seismology, for which the main concern is shear rupture on a fault, Kame & Yamashita (1999a,b) developed the BIEM for a mode II crack based on a different formulation and investigated shear crack bending and branching. An outstanding advantage of the BIEMs is that there are no directional constraints on a crack tip path.

Kame & Yamashita (1999a,b) simulated the spontaneous growth of a mode II crack in which the propagation path is dynamically self-chosen. Their simulation showed exactly those high off-plane stresses at the crack tip as predicted in the previous theoretical solution. They base the choice of the orientation of each new increment of crack path on the maximum hoop shear stress very near the crack tip, explicitly including the high-speed distortion of the stress field. They consider growth of a frictionless crack in a medium with uniform pre-stress and fracture strength. The results show that when a high speed is attained, the crack tip bifurcates and each branch bends symmetrically, so much so that the rupture ultimately arrests: the bent paths encouraged by off-plane stressing very near the tip are discouraged by the larger-scale pre-stress. They gave a new insight into the arresting mechanism of earthquake faulting, in that rupture growth could be arrested spontaneously due to self-radiating waves by means of bending without recourse to any heterogeneities in the pre-stress state and/or the fracture strength.

Following the previous work of Kame & Yamashita (1999a,b), here we further investigate additional areas of mode II rupture propagation in a self-chosen crack path model. We again simulate the spontaneous growth of a crack without constraints on the path. In this paper, we introduce Coulomb friction on the rupture surface and first investigate how the friction affects the rupture path. It will be shown that after bifurcation of the crack tip into two branches each branch grows asymmetrically due to different friction levels. The resulting rupture trace is seemingly paradoxical from the point of view of the friction level: branching in the compressional side finally dominates even though higher friction acts on it. We will see how such a trace is dynamically formed under the action of Coulomb friction and also see that it is consistent with the observed active fault traces. Then we synthesize the waveforms to find distinctive phases associated with the dynamic branching. We compare them with those emitted by two planar crack models for which the growths are arrested by inhomogeneities in the fracture strength or the pre-stress. We will see what part of the branching process will and will not contribute to the waveforms significantly.

2 NUMERICAL METHOD AND MODEL CONFIGURATION

2.1 Boundary integral equation method

We use the elastodynamic boundary integral equation method proposed by Kame & Yamashita (1999b) to allow simulations of rupture in which the rupture path is dynamically self-chosen. In the BIEM, the incremental tractions caused by a crack are represented in terms of the slip-rate history. We can evaluate the tangential and normal incremental tractions, $\Delta T_t(\varphi)$ and $\Delta T_n(\varphi)$, at a point on an arbitrarily inclined crack element at each time step, where the angle φ represents an angle measured counter-clockwise from the x_1-axis. Applying a discretization where a constant slip velocity V_t is assumed within each spatial grid (Δs) during each time step (Δt), we can briefly write the BIE in the following symbolic form:

$$\Delta T_t^{ln} = K_t^{00:00} V_t^{ln} + \sum_{k=0}^{n-1} \sum_i K_t^{ln:ik} V_t^{ik}, \tag{1}$$

where l and i represent the discretized position on the crack and n and k represent the discretized time step. Here we assume that the crack surfaces are closed everywhere, i.e. the displacement discontinuity on the crack only has a tangential (purely mode II) component. The first term $K_t^{00:00}$ on the right-hand side is called the instantaneous stress term (Cochard & Madariaga 1994), which represents the instantaneous contribution of the current slip velocity to the traction at the same position. The second term contains the contribution of the past slip-rate history; $K_t^{ln:ik}$ indicates the tangential stress kernel at (l, n) due to unit slip velocity at (i, k). The normal component ΔT_n^{ln} has a similar symbolic form except that its instantaneous term equals zero as long as we consider no opening slip on a crack. In order to determine the traction ΔT_t^{ln} and the slip velocity

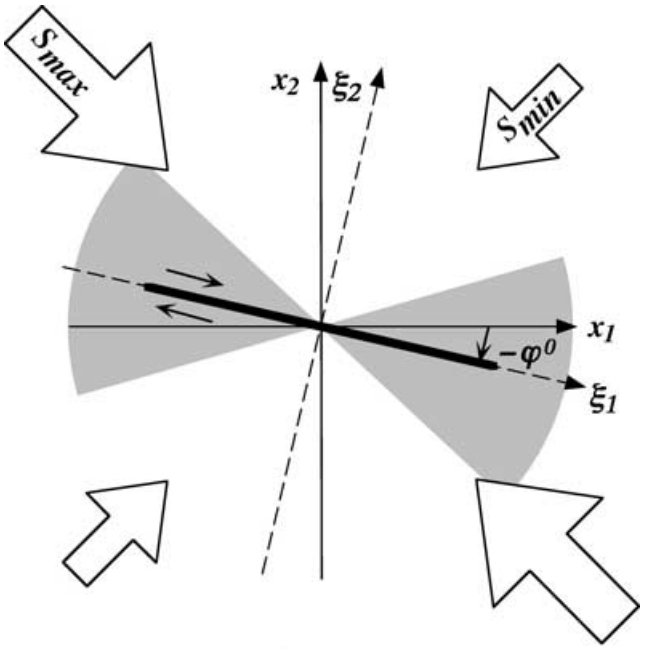

Figure 3. Configuration of the biaxial compression and the seed crack. The grey region indicates the angle range within which the applied stresses can be released against Coulomb friction on a planar crack with right-lateral slip.

$V_{\rm t}^{ln}$ at a current time step, we solve eq. (1) under the imposed boundary condition. Once the slip-rate history on the crack is obtained through a simulation, the displacement velocity at an arbitrary point can be calculated from similar discretized forms (e.g. Kame & Yamashita 1997 for the mode III case; Tada & Madarigaga 2001 for all modes).

2.2 Biaxial compression as an externally applied load

Earthquake faulting is modelled as dynamic growth of a mode II crack in an infinite homogeneous isotropic elastic medium. The medium is subjected to biaxial compression ($S_{\rm max} < S_{\rm min} < 0$, we take tension as positive) as illustrated in Fig. 3. We take a Cartesian coordinate (x_1, x_2) and the direction of compression is set at an angle 45° from the axis. We take this biaxially compressed state without cracks as a pre-stress state. Shear and normal tractions acting on a φ inclined plane under the pre-stress state are represented as $T_{\rm t}^0(\varphi) = \tau^0 \cos 2\varphi$ and $T_{\rm n}^0(\varphi) = \sigma^0 - \tau^0 \sin 2\varphi$, where $\tau^0 = (S_{\rm min} - S_{\rm max})/2 > 0$, $\sigma^0 = (S_{\rm max} + S_{\rm min})/2 < 0$.

2.3 Coulomb's law of friction

We introduce Coulomb's law of friction to describe frictional force on a crack surface. The friction level T_f is given by a dynamic frictional coefficient f multiplied by the total normal traction,

$$T_f = f \times (-T_{\rm n}), \tag{2}$$

where the total traction is a sum of the pre-stress traction and the incremental traction ($T_{\rm n} = T_{\rm n}^0 + \Delta T_{\rm n}$). In this paper, this friction coefficient is the same all over the crack branches and the total normal traction is the only factor that alters the friction level. If a planar crack is considered, it never alters the total normal traction on itself. Otherwise the total normal traction does change and we have to note that this analysis is such a non-planar crack case.

This study is an extension of a number of earlier analyses of bend/branch instabilities in in-plane cracks at the high-speed propagation stage (Yoffe 1951; Freund 1989; Koller *et al.* 1992). Accordingly we base our simulations on a crack model with no strength-weakening zone behind the tip. When we consider no process zone, the shear traction suddenly drops to the dynamic friction level behind the crack tip.

We introduce a static planar seed crack with right-lateral slip prior to dynamic nucleation at the crack tips and take a local coordinate (ξ_1, ξ_2) along it (Fig. 3). Assuming that the plane of the seed crack coincides with the most likely direction expected from the Mohr circle for the pre-stress level, we obtain the angle φ^0 (e.g. Mogi 1974) as

$$\varphi^0 = -\frac{1}{2} \tan^{-1} f. \tag{3}$$

In the following simulation, the friction coefficient is presumed to be $f = 0.488$ and the angle is $\varphi^0 = -13°$. Note that φ^0 is the most favourable angle for the right-lateral slip against the friction at which the stress drop function

$$\Delta\sigma(\varphi) \equiv T_{\rm t}^0(\varphi) - T_f(\varphi) \tag{4}$$

takes the maximum. Spontaneous rupture will be encouraged only within a range where the stress drop function is positive. The range depends both on the differential stress $|S_{\rm max} - S_{\rm min}|$ and the frictional coefficient f. The narrower range is expected for the larger f and/or the smaller differential stress. If we consider a simple case of a planar crack where the total normal coincides with the pre-stress normal, the range is approximately $-41° < \varphi < +15°$ for the pre-stress state used in the following simulation. This corresponds to ±28° and is symmetric with respect to the optimum angle $\varphi^0 = -13°$ (Fig. 3).

2.4 Procedure for spontaneous crack growth

As we assume a crack model with no strength-weakening zone behind the tip, the crack inevitably has a square-root stress singularity at the tip. In a framework of linear fracture mechanics, a stress intensity factor is introduced to handle this singularity and is used for the determination of crack tip extension (Irwin 1958). The critical stress fracture criterion we employed here is a numerical implementation of a critical stress intensity factor criterion (e.g. Das & Aki 1977; Virieux & Madariaga 1982). It is often a problem that stress evaluated numerically at the tip is dependent on the grid spacing because of the singularity. When the grid size is fixed, however, the critical stress criterion is approximately equivalent to the stress intensity factor-based criterion (Das & Aki 1977).

Using the elastostatic BIEM (Kame & Yamashita 1999b), we first determine the static slip distribution on the seed crack in a state of equilibrium and then calculate the hoop shear concentration $\Delta T_{\rm t}(\varphi = \varphi^0)$ at the tip. We assume that the critical fracture strength $T_{\rm c}$ of the medium is slightly smaller than $\Delta T_{\rm t}(\varphi = \varphi^0)$ in order to nucleate the dynamic growth.

We employ a hoop shear maximization criterion as a criterion for the crack tip extension direction (Koller *et al.* 1992; Kame & Yamashita 1999a,b). At the *n*th time step, the angular distribution of incremental hoop shear traction $\Delta T_{\rm t}(\varphi)$ is calculated ahead of the crack tip in a range $\varphi_{n-1} - 90° < \varphi < \varphi_{n-1} + 90°$ every 1°, where φ_{n-1} is the tip angle at the preceding time step measured counterclockwise from the x_1-axis. The evaluation point for tractions is $\Delta s/2$ ahead of the tip (Fig. 1). Then we search for the maximum value $\Delta T_{\rm t}(\varphi)$ and its direction $\varphi_{\rm n}$. If $\Delta T_{\rm t}(\varphi_{\rm n})$ exceeds the critical fracture strength of the medium $T_{\rm c}$, the tip is assumed to extend by

one element in the direction φ_n. We then determine the slip velocity on the crack by using eqs (1), (2) and (4). In order to suppress short-wavelength oscillation in the slip velocity we introduce an artificial damping term in the same way as in Yamashita & Fukuyama (1996) and Kame & Yamashita (1999b).

2.5 Numerical unit

Our computations are made using the following non-dimensional quantities:

$$\Delta T' = \Delta T/\Delta\sigma(\varphi^0), \quad V_t' = V_t/c_d, \quad x' = x/\Delta s, \quad t' = tc_d/\Delta s. \tag{5}$$

We assume $c_d/c_s = \sqrt{3}$, a Poisson solid, where c_d and c_s are the dilatational and shear wave speeds. We choose the discretization intervals so that $c_d\Delta t/\Delta s = \frac{1}{2}$. We base the normalization on the stress drop on the seed crack, the grid size and double the time step. The prime symbol is omitted in the following for simplicity.

3 SIMULATION OF SPONTANEOUS CRACK GROWTH UNDER THE EFFECT OF COULOMB FRICTION

We now investigate the spatio-temporal evolution of a spontaneously growing crack on which Coulomb friction acts. We assume an ideal condition that the pre-stress state and the fracture strength T_c is homogeneous over the medium in order to elicit the effects of wave stresses and Coulomb friction on the path. The initial length of a seed crack is assumed to be $l_0 = 5$ and the critical fracture strength is correspondingly determined as $T_c = 1.21$. These parameters are the same as assumed in Kame & Yamashita (1999b), in which frictionless cases were investigated. The friction coefficient is $f = 0.488$ and the optimum angle for the seed crack is $\varphi^0 = -13^\circ$. To take the stress drop on it as unity, the biaxial compression is set to $S_{max} = -4.30$ and $S_{min} = -0.430$. On the seed crack, the externally applied stress is not released totally due to friction. The residual level T_f is approximately 43 per cent of the applied shear traction $T_t^0(\varphi^0)$. The nucleation is assumed to occur at $t = 0.0$.

Fig. 4 shows the snapshots of rupture growth and the corresponding incremental hoop shear distribution. The hoop shear traction takes its maximum in the direction of the original crack plane at $t = 0.0$, i.e. the crack begins its growth along the original plane. The crack growth accelerates soon after the nucleation, and the crack velocity attains a value of $0.76c_s$ at $t = 8.0$. The maximum shear axis still remains on the original crack plane, the crack accordingly grows further straight on. At $t = 15.5$, the velocity attains $0.87c_s$ and the maximum shear exceeds the fracture strength off the plane for the first time. This velocity is measured to be slightly larger than the theoretically predicted one $c_{crt} = 0.77c_s$ because of insufficient resolution of rupture velocity against spatio-temporally discrete crack propagation. The directions deviate from the original plane by $\pm 42^\circ$, i.e. $+29^\circ$ and -55° with respect to the x_1-axis, respectively. At this high-speed propagation stage, the crack tip is bifurcated symmetrically with respect to the initial crack plane into two branches due to stress waves localized around the crack tip. Each of the two branches is generated in compressional and tensile stress regions around the propagating tip as marked by $+$ and $-$, respectively, in Fig. 4. The bending increases with a larger rate for the branch in the tensile stress region (turning to the directions -55°, -87° at $t =$ 15.5, 16.5, respectively). On the other hand, the increasing rate of bending is smaller in the compressional stress region ($+29^\circ$, $+13^\circ$, $+16^\circ$, $+21^\circ$ at $t = 15.5, 21.5, 23.5, 29.5$). The difference of bending rates can be attributed to the different friction levels on them. The resistance to the slip is lower in the tensile stress region because lower friction is acting there, so that a stress wave favourable for bending is radiated more from the branch in the tensile side and vice versa. We think this is why the bending rate is higher for the tensile side branch. In contrast to the frictionless model (model B in Kame & Yamashita 1999b), an asymmetrical branching path is formed under the effect of Coulomb friction. It is in principle allowed by our method that a branch further branches. However, this does not occur in the model because once branching occurs the rupture velocity of each branch tip begins to decelerate and never becomes high enough to emit sufficient wave stress to make bifurcation begin again.

Under biaxial compression, bending larger than a critical threshold leads to negative stress drop on the curved crack branch. A negative stress drop brings down the stress concentration at the tip, which never exceeds the critical value (see the hoop shear distributions around the both tips at $t = 44.5$ a while after the final crack-tip growth at $t = 29.5$). The branch in the compressive side can grow more because the negative stress drop on that shallow bending surface is not so large as to terminate rupture growth immediately. This result contradicts the presumption in the frictionless case (model C in Kame & Yamashita 1999b) that crack propagation will be easier in the tensile side because of virtual friction. Our analysis is an example that such an intuitive presumption does not hold when we consider a dynamic bending process. Either way, the branch paths encouraged by off-fault stressing very near the tip are discouraged by the larger-scale pre-stress as pointed out in Kame & Yamashita (1999a,b).

It has been pointed out that surface traces of active faults tend to bend in a direction where the frictional force is larger (Matsuda 1967). The geodetically estimated varied fault trace of the 1943 Tottori earthquake also shows a fine compressional side bending at both ends (Kanamori 1972). However, the mechanism of bending in the compressional side remained unclear because slip is thought to be easier to occur on the extensional side than in the compressional side based on Coulomb friction levels on branches. The dynamic process we showed here can naturally explain the observed tendency of fault bend to dominate on the compressional side: after dynamic bifurcation, lower friction on the branch in the tensile side leads to a larger rate for bending that results in a quicker arresting of its growth and vice versa. An apparently paradoxical bending direction can be, in fact, a natural result of a dynamic branching process under the effect of Coulomb friction.

4 ELASTIC WAVE RADIATION DUE TO BRANCHING AND ARRESTING

In this section, we synthesize the velocity waveforms of the 'branching model' in the preceding section in order to find phases associated with dynamic branching and arresting. For this purpose, we compare them with those radiated by two other models in which rupture is arrested remaining on the original planar plane: the 'sudden stopping model' and the 'gradual stopping model'. In the 'sudden stopping model', we assume that the pre-stress state is uniform and rupture is suddenly arrested when the crack tips reach high strength regions called barriers. The barrier regions are assumed on $|\xi_1| \geq$ 10.5. In the 'gradual stopping model', we assume that the strength is uniform, however, the pre-stress state is inhomogeneous. We consider stress-drop decreasing regions where spontaneous growth of rupture is gradually but finally discouraged. The stress drop $\Delta\sigma$ is presumed to decrease linearly between $|\xi_1| = 5.5$ and 10.5 from 1.0 to -0.25 and keeps a negative value $\Delta\sigma = -0.25$ on $|\xi_1| \geq 10.5$.

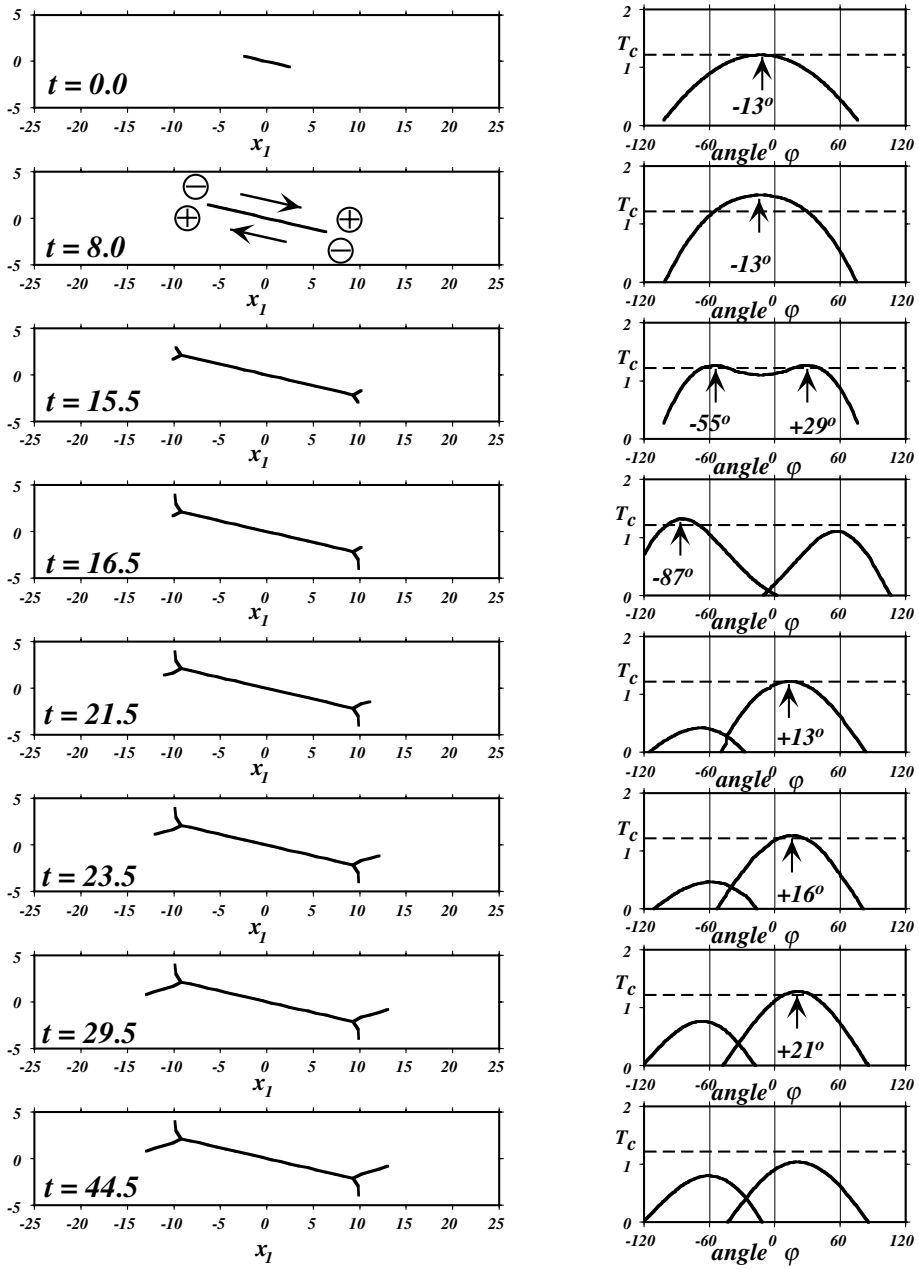

Figure 4. Snapshots of the model. The right-hand column represents the angular distribution of the hoop shear traction corresponding to the left column. The arrows indicate the angles at which the maximum hoop shear exceeds T_c. Marks + and − indicate the incrementally compressional and tensile stress regions, respectively.

We assume the same condition for the pre-stress and the fracture strength around a seed crack in each model and inhomogeneous regions are chosen so that the total moments released in the three models become approximately the same.

We first show spatio-temporal evolution of the crack tip positions (Fig. 5). The crack tip of the 'sudden stopping model' increases the rupture speed monotonically after nucleation and is arrested suddenly after reaching the rupture speed $v_r = 0.87c_s$ at the barrier $\xi_1 = 10.5$. On the other hand, that of the 'gradual stopping model' accelerates up to $v_r = 0.87c_s$ and then decelerates gradually after entering the negative stress-drop region and finally stops at $\xi_1 = 16.5$. In the 'branching model', rupture on the original plane bifurcates at $\xi_1 = 9.5$ and then transfers into two branches. The tip in the tensile side stops first and that in the compressional side stops after a while. The positions of the final tips are $\xi_1 = 10.14$ and 12.39, respectively, where they are measured after projecting on to the ξ_1-axis.

The synthesized velocity waveforms radiated from these three rupture processes are shown in Fig. 6. The observation point is (ξ_1, ξ_2) = (25, 0). We first compare the waveforms of the 'branching model' and the 'sudden stopping model' in the transverse (ξ_2) component (Fig. 6a). The onset is at $t = 21.5$, which corresponds to the arrival of the nucleation phase. In the 'sudden stopping model', the rupture duration time is 16.5 and stopping information accordingly arrives around $t = 38.0$. It corresponds to a time when the velocity waveform begins to turn around. We can find that both models show little difference. The reason is this: the slip velocities of both models are almost the same on the original planar plane and they contribute

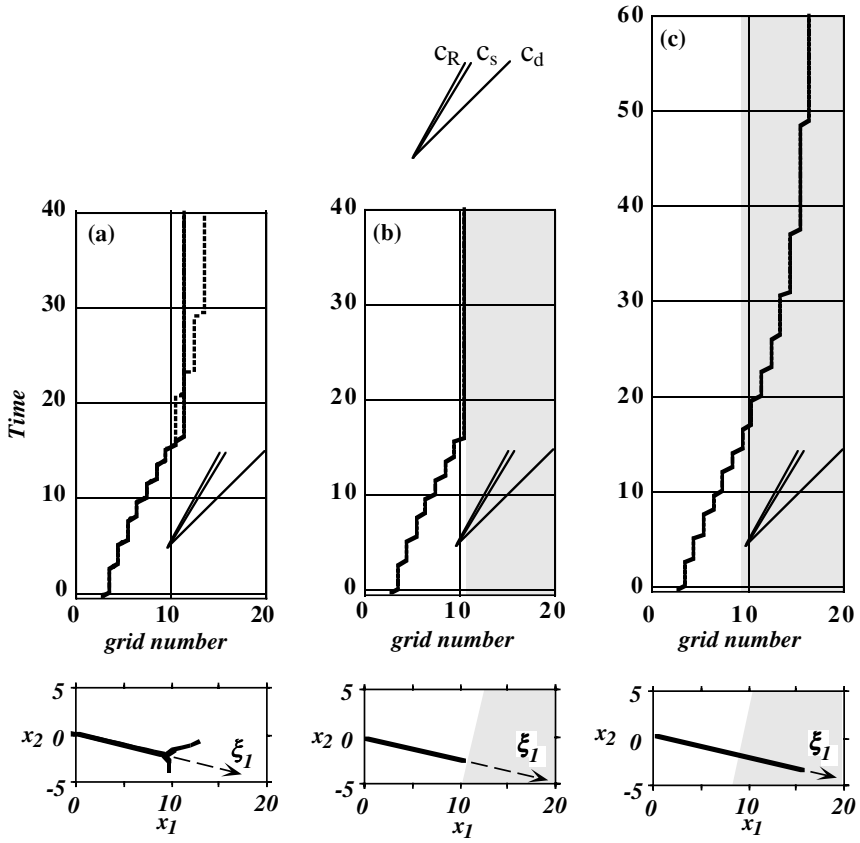

Figure 5. Spatio-temporal plot of the propagating tips of (a) the branching model, (b) the sudden stopping model and (c) the gradual stopping model. The lower figures show their final traces. The dotted line in (a) indicates the branch tip in the compressional side. The grey regions indicate the barrier regions in (b) and the negative stress-drop regions in (c). The Rayleigh c_R, the shear c_s and the dilatational c_d wave speeds are also plotted for reference.

to the waveforms the most. On the other hand, the slip velocity on branches in the 'branching model' is negligible due to a negative stress drop so that they cannot make a little contribution to the waveform. The branching process itself contributes to sudden arresting of rupture on the original plane, which brings a sharp waveform around $t = 42.0$ rich in high frequencies similar to the 'sudden stopping model'. Sudden arresting of rupture is known as one of the major sources for radiating high-frequency waves (Madariaga 1977). In the 'branching model', such a discontinuous rupture stopping is caused by self-radiating wave stresses even without any inhomogeneity in the fracture strength or the pre-stress.

Then we see the waveforms in the radial (ξ_1) component (Fig. 6b). Note that the observation point is on ξ_1-axis that is a nodal plane for mode II ruptures where no radial waves are expected by the planar models. Thus, we can find a branching phase unless its amplitude is zero. Regardless of the small slip velocity on branches, we can certainly see a slight weak phase directly associated to dynamic branching. We see that the branching phase is so weak that it cannot be identified in the transverse component. From a waveform point of view, the 'branching model' is practically equivalent to the 'sudden stopping model'.

The transverse (ξ_2) component of waveforms of the 'branching model' and the 'gradual stopping model' is plotted in Fig. 6(c). Here we can recognize a clear difference between the two. The 'gradual stopping model' has a lower and wider peak around $t = 42.0$ than the 'branching model'. The difference can be attributed to the different way of rupture arresting: a rupture gradually decelerates to stop after entering into the negative stress-drop region in the 'gradual stopping model'. This means the waveform contains a smaller high-frequency component than the 'branching model'.

After all, we could not find a distinctive phase associated with dynamic branching. These results lead us to a general idea for radiation of seismic waves on a branched fault: if the planar part of the branched fault is inclined at an optimum angle for a frictional slip with respect to a remotely applied pre-stress, we can expect little wave radiation from the branching parts of the fault. This is because an insignificant stress drop will occur on them. This gives the pessimistic view that kinematic inversion analyses using observed waveform data of large events that often are followed by surface branching/bending traces, are helpless in detecting branch structure underground. At the same time, we could find the significant effect of the branching process on high-frequency wave radiation. Because dynamic branching occurs at the high-speed propagation stage and then results in a sudden arresting of rupture on the original plane, it can be a major source for high-frequency radiation as expected in the theoretical study of a planar faulting (Madariaga 1977). High-frequency wave radiation by dynamic branching is a novel idea in that it is a self-excited phenomenon due to high off-plane stressing at high-speed propagation without recourse to any strong heterogeneities in the fracture strength and/or the pre-stress state assumed in classical planar rupture models.

5 DISCUSSIONS AND CONCLUSIONS

We investigated mode II shear crack growth in which rupture path is dynamically self-chosen. The simulations were implemented using

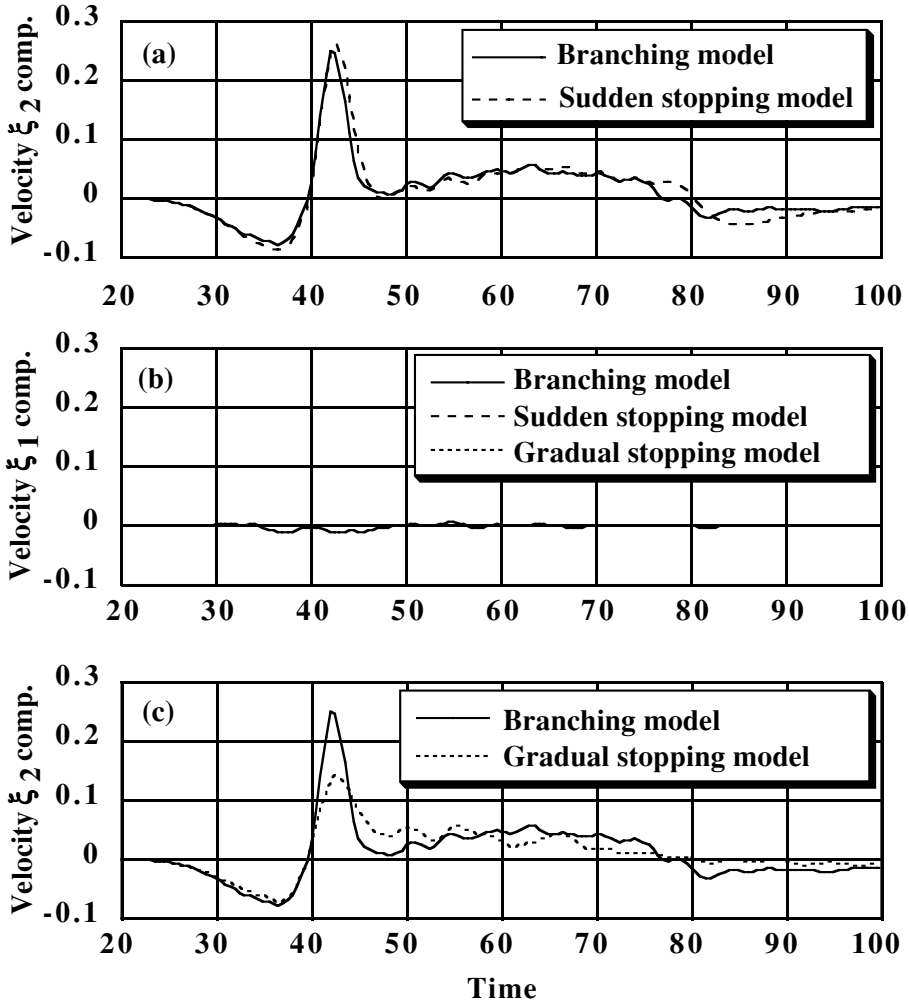

Figure 6. Comparison of the synthesized velocity waveforms of three models. Low-pass filtering of the original data is done at non-dimensional frequency 0.10. (a) Transverse (ξ_2) component of the velocity waves radiated by the 'branching model' and the 'sudden stopping model'. (b) Radial (ξ_1) component of all the three models. (c) Transverse (ξ_2) component of the velocity waveforms of the 'branching model' and the 'gradual stopping model'.

the boundary integral equation method proposed by Kame & Yamashita (1999b), which does not impose any constraints on the crack tip path. We considered a crack in an unbounded medium under biaxial compression. The crack tip was assumed to extend dynamically in the direction where the incremental hoop shear traction takes its maximum and exceeds the fracture strength.

First, we investigated rupture paths under the effects of wave stresses and Coulomb friction. Our simulation showed that the crack spontaneously bifurcates due to high off-plane stresses at the high-speed propagation stage. The branches increase their angles asymmetrically due to different friction levels acting on them. Finally, the branch in the compressional side grows more than that in the tensile side. Either way, the branch paths nucleated by off-fault stressing very near the tip are arrested by the larger-scale pre-stress. Though the resultant trace is apparently paradoxical in terms of friction level, it is dynamically reasonable and is consistent with field observations of active faults. The ratio of the branched segment to the planar part of the crack is approximately 20 per cent in the simulation, which is larger than those in observed traces. In our modelling, the ratio will be smaller for smaller friction coefficient f and/or a larger differential stress $|S_{\max} - S_{\min}|$ encouraged by the high rate of bending.

Then we synthesized the waveform to find distinctive phases associated with dynamic branching. We could not find any significant branching phases in comparison with waveforms of planar rupture models for which rupture is arrested by strong heterogeneities in the pre-stress or the fracture strength. We deduce from this that the curved branches are less efficient for wave radiation than the planar part of the crack. On the other hand, we found that dynamic branching can be a radiation source of high-frequency waves because of a significant discontinuity in the rupture velocity on the original planar plane. Our result gives a new insight into the dynamics of high-frequency seismic wave radiation: a high-frequency wave can be radiated in a self-excited dynamic process due to high off-plane stressing without recourse to any strong inhomogeneities in the pre-stress state and/or the fracture strength.

There is a certain model-specific assumption concerning crack growth: we implicitly prohibit re-nucleation of arrested rupture on the original plane after bifurcation. This is because the order of stress singularity produced in the vicinity of the branch point is lower than that at the crack tip. This means that no rupture is expected to nucleate at the branch point after the termination of rupture growth so long as a singular crack is assumed. If a finite stress model such as a slip-weakening model (Ida 1972; Palmer & Rice 1973) is assumed,

the stress in the vicinity of a branch point can be higher than that at the crack tip; hence, rupture can re-nucleate at a branch point in such a case after the termination of rupture growth.

If we consider a finite stress crack, a finite strength-weakening zone is inevitably accompanied behind the tip (Ida 1972; Palmer & Rice 1973). If a strength-weakening zone were present, the stress concentration in the vicinity of the rupture front would be diffused in a different way (Poliakov *et al.* 2002). In addition, pre-stress will also be directly related to the hoop stress distribution around the crack tip. A dynamically self-chosen rupture path has to also be investigated in a finite stress model including re-nucleation of rupture after branching in further simulations. In this case, rupture nucleation should be allowed not only for rupture ends, but also allowed wherever stress exceeds a finite threshold value. Some researchers have investigated what rupture path is dynamically self-chosen on a branched fault system allowing re-nucleation with such a finite stress model (Aochi *et al.* 2000, 2002; Aochi & Fukuyama 2002; Kame *et al.* 2003), though rupture is only allowed on the prescribed paths.

We successfully showed that dynamically excited off-plane stressing can make a non-planar rupture path that does control the dynamic process including branching of the rupture, its arresting and the elastic wave radiation. Dynamically self-chosen crack path modelling gave us a profound understanding of the rupture dynamics. Using this modelling, we will have a set of interesting problems in earthquake fracture dynamics. One example is dynamic interaction among cracks. The crack traces are expected to be strongly affected by waves reflected from each crack surface. In a matured fault zone where lots of cracks are expected to exist, off-fault stressing should contribute to either self-arresting of a single crack or activation of other cracks accompanied by off-plane coalescence. This will give a new way of thinking about the origin of small earthquakes and the frequency–magnitude relation, because it provides a way to stop and continue ruptures without recourse to assuming strong heterogeneity along the fault zone itself. This paper is just a start and will trigger a number of challenging problems in the physics of earthquakes.

ACKNOWLEDGMENTS

NK was supported primarily by JSPS Postdoctoral Fellowship for Research Abroad 2000–2002, and by MEXT Grant-in-Aid for Young Scientists (B) 15740277. The work was additionally supported by RR2002 MEXT grant to NK on 'Regional characterization of the crust in metropolitan areas for prediction of strong ground motion', and by ERI grant to NK and TY for collaboration 2003-G-22. We appreciate reviews of the manuscript by Raul Madariaga, Alain Cochard and an anonymous reviewer.

REFERENCES

Aochi, H. & Fukuyama, E., 2002. Three-dimensional nonplanar simulation of the 1992 Landers earthquake, *J. geophys. Res.,* **107,** (B2), doi:10.129/2000JB000061.

Aochi, H., Fukuyama, E. & Matsu'ura, M., 2000. Selectivity of spontaneous rupture propagation on a branched fault, *Geophys. Res. Lett.,* **27,** 3635–3638.

Aochi, H., Madariaga, R. & Fukuyama, E., 2002. Effect of normal stress during rupture propagation along nonplanar faults, *J. geophys. Res.,* **107,** (B2), doi:10.129/2001JB000500.

Barka, A., 1999. The 17 August 1999 Izmit earthquake, *Science*, **285,** 1858–1859.

Cochard, A. & Madariaga, R., 1994. Dynamic faulting under rate-dependent friction, *Pure appl. Geophys.,* **142,** 419–445.

Das, S. & Aki, K., 1977. A numerical study of two-dimensional spontaneous rupture propagation, *Geophys. J. R. astr. Soc.,* **50,** 643–668.

Felzer, K.R. & Beroza, G., 1999. Deep structure of a fault discontinuity, *Geophys. Res. Lett.,* **26,** 2121–2124.

Freund, L.B., 1989. *Dynamic Fracture Mechanics,* pp. 170–175, Cambridge University Press, Cambridge.

Ida, Y., 1972. Cohesive force across the tip of a longitudinal-shear crack and Griffith's specific surface energy, *J. geophys. Res.,* **77,** 3796–3805.

Irwin, G.R., 1958. Fracture mechanics, in *Handbuch der Physik,* Vol. 79, pp. 551–590, Springer-Verlag, Berlin.

Kame, N. & Yamashita, T., 1997. Dynamic nucleation process of shallow earthquake faulting in a fault zone, *Geophys. J. Int.,* **128,** 204–216.

Kame, N. & Yamashita, T., 1999a. A new light on arresting mechanism of dynamic earthquake faulting, *Geophys. Res. Lett.,* **26,** 1997–2000.

Kame, N. & Yamashita, T., 1999b. Simulation of spontaneous growth of dynamic crack without constraints on the crack tip path, *Geophys. J. Int.,* **139,** 345–358.

Kame, N., Rice, J.R. & Dmowska, R., 2003. Effects of prestress state and rupture velocity on dynamic fault branching, *J. geophys. Res.,* **108,** (B5), 2265, doi:10.1029/2002JB002189.

Kanamori, H., 1972. Determination of effective tectonic stress associated with earthquake faulting, the Tottori Earthquake of 1943, *Phys. Earth planet. Inter.,* **5,** 426–434.

King, G. & Nabelek, J., 1985. Role of fault bends in the initiation and termination of earthquake rupture, *Science,* **228,** 984–987.

Koller, M.G., Bonnet, M. & Madariaga, R., 1992. Modelling of dynamical crack propagation using time-domain boundary integral equations, *Wave Motion,* **16,** 339–366.

Madariaga, R., 1977. High-frequency radiation from crack (stress drop) models of earthquake faulting, *Geophys. J. R. astr. Soc.,* **51,** 625–651.

Massonnet, D., Rossi, M., Carmona, C., Adragna, F., Peltzer, G., Feigl, K. & Rabaute, T., 1993. The displacement field of the Landers earthquake mapped by radar interferometry, *Nature,* **364,** 138–142.

Matsuda, T., 1967. Geology of earthquake faults (in Japanese), *Zisin,* **20,** 230–235.

Mogi, K., 1974. On the pressure dependence of strength of rocks and the coulomb fracture criterion, *Techtonophysics,* **21,** 273–285.

Palmer, A.C. & Rice, J.R., 1973. The growth of slip surfaces in the progressive failure of overconsolidated clay, *Proc. R. Soc. Lond. A,* **332,** 527–548.

Poliakov, A.N., Dmowska, R. & Rice, J.R., 2002. Dynamic shear rupture interactions with fault bends and off-axis secondary faulting, *J. geophys. Res.,* **107,** (B11), 2295, doi:10.1029/2001JB000572.

Rice, J.R., 1980. The mechanics of earthquake rupture, in *Physics of the Earth's Interior, Proc. International School of Physics 'Enrico Fermi',* pp. 555–649, eds Dziewonski, A.M. & Boschi, E., Italian Physics Society and North-Holland, Amsterdam.

Sieh, K. *et al.,* 1993. Near-field investigations of the Landers Earthquake sequence, April to July, 1992, *Science,* **260,** 171–176.

Seelig, Th. & Gross, D., 1999. On the interaction and branching of fast running cracks—a numerical investigation, *J. Mech. Phys. Solids,* **47,** 935–952.

Tada, T. & Madariaga, R., 2001. Dynamic modelling of the flat 2-D crack by a semi-analytic BIEM scheme, *Int. J. Numer. Meth. Eng.,* **50,** 227–251.

Umeda, Y., 1990. High-amplitude seismic waves radiated from the bright spot of an earthquake, *Tectonophysics,* **175,** 81–92.

Virieux, J. & Madariaga, R., 1982. Dynamic faulting studied by a finite difference method, *Bull. seism. Soc. Am.,* **72,** 345–369.

Xu, X.P. & Needleman, A., 1994. Numerical simulations of fast crack growth in brittle solids, *J. Mech. Phys. Solids,* **42,** 1397–1434.

Yamashita, T. & Fukuyama, E., 1996. Apparent critical slip displacement caused by the existence of a fault zone, *Geophys. J. Int.,* **125,** 459–472.

Yoffe, E.H., 1951. The moving Griffith crack, *Phil. Mag.,* **42,** 739–750.

Yoshida, S., Koketsu, K., Shibazaki, B., Sagiya, T., Kato, T. & Yoshida, Y., 1996. Joint inversion of near- and far-field waveforms and geodetic data for the rupture process of the 1995 Kobe earthquake, *J. Phys. Earth,* **44,** 437–454.

APPENDIX: ELASTODYNAMIC SINGULAR CRACK SOLUTION

For mode II deformation, the incremental hoop traction distribution near a running crack tip at a speed of v_r has the following form:

$$\Delta T_i(\varphi) = \frac{K_{\rm II}}{\sqrt{2\pi r}} F_i^{\rm II}(\varphi, v_r) + o(1) \quad \text{as} \quad r \to +0, \tag{A1}$$

where $K_{\rm II}$ is the mode II stress intensity factor at the moment and the subscript i will either be 't' denoting tangential or 'n' denoting a normal component.

The stress components due to the running crack on x_1-axis with stress drop $\Delta\sigma$ are

$$\Delta\tau_{11} = -\frac{K_{\rm II}}{\sqrt{2\pi r}} \frac{2\alpha_s}{D} \times \left[\left(1 + 2\alpha_d^2 - \alpha_s^2\right) \frac{\sin(\theta_d/2)}{\sqrt{\gamma_d}} - \left(1 + \alpha_s^2\right) \frac{\sin(\theta_s/2)}{\sqrt{\gamma_s}} \right], \tag{A2}$$

$$\Delta\tau_{22} = \frac{K_{\rm II}}{\sqrt{2\pi r}} \frac{2\alpha_s \left(1 + \alpha_s^2\right)}{D} \left[\frac{\sin(\theta_d/2)}{\sqrt{\gamma_d}} - \frac{\sin(\theta_s/2)}{\sqrt{\gamma_s}} \right], \tag{A3}$$

$$\Delta\tau_{12} = \frac{K_{\rm II}}{\sqrt{2\pi r}} \frac{1}{D} \times \left[4\alpha_d\alpha_s \frac{\cos(\theta_d/2)}{\sqrt{\gamma_d}} - \left(1 + \alpha_s^2\right)^2 \frac{\cos(\theta_s/2)}{\sqrt{\gamma_s}} \right] - \Delta\sigma \quad \text{as} \quad r \to +0 \tag{A4}$$

(Freund 1989; Poliakov *et al.* 2002). Here $\alpha_j = \sqrt{1 - (v_r/c_j)^2}$, $D = 4\alpha_d\alpha_s - (1 + \alpha_s^2)^2$, $\gamma_j = \sqrt{1 - (v_r \sin\varphi/c_j)^2}$, $\theta_j = \tan^{-1}(\alpha_j \tan\varphi)$, where the variable α, γ, θ will have either 'd' or 's' as a subscript. The above equations are used for plotting $F_t^{\rm II}$ (φ, v_r) in Fig. 2. They are also used for finding the 'critical speed' $v_{\rm crt}$ across which the hoop maximum shift from the original plane to off-plane.